JACS
JOURNAL OF THE AMERICAN CHEMICAL SOCIETY
pubs.acs.org/JACS
Article

Further Dimensions for Sensing in Biofluids: Distinguishing Bioorganic Analytes by the Salt-Induced Adaptation of a Cucurbit[7]uril-Based Chemosensor

Changming Hu, Thomas Jochmann,* Papri Chakraborty, Marco Neumaier, Pavel A. Levkin, Manfred M. Kappes,* and Frank Biedermann*

Cite This: J. Am. Chem. Soc. 2022, 144, 13084−13095
Read Online
ACCESS | Metrics & More | Article Recommendations | Supporting Information

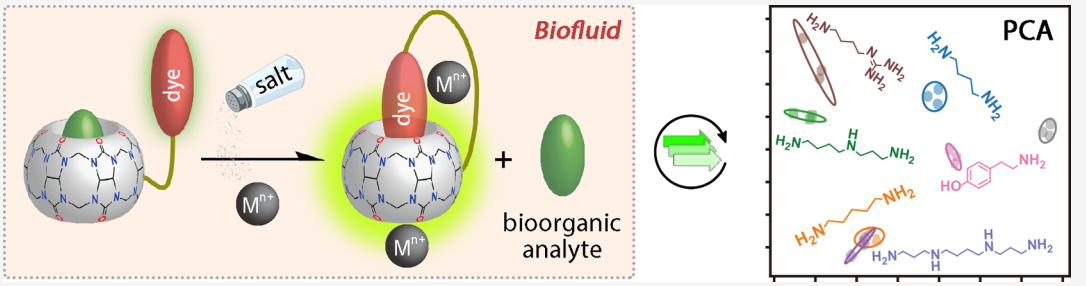

ABSTRACT: Insufficient binding selectivity of chemosensors often renders biorelevant metabolites indistinguishable by the widely used indicator displacement assay. Array-based chemosensing methods are a common workaround but require additional effort for synthesizing a chemosensor library and setting up a sensing array. Moreover, it can be very challenging to tune the inherent binding preference of macrocyclic systems such as cucurbit[*n*]urils (CB*n*) by synthetic means. Using a novel cucurbit[7]uril-dye conjugate that undergoes salt-induced adaptation, we now succeeded in distinguishing 14 bioorganic analytes from each other through the facile stepwise addition of salts. The salt-specific concentration-resolved emission provides additional information about the system at a low synthetic effort. We present a data-driven approach to translate the human-visible curve differences into intuitive pairwise difference measures. Ion mobility experiments combined with density functional theory calculations gave further insights into the binding mechanism and uncovered an unprecedented ternary complex geometry for CB7. TThis work introduces the non-selectively binding, salt-adaptive cucurbit[*n*]uril system for sensing applications in biofluids such as urine, saliva, and blood serum.

INTRODUCTION

Synthetic receptors and chemosensing ensembles capable of distinguishing structurally similar bioorganic analytes are crucial for developing facile, low-cost, and parallelizable sensing methods that are applicable in molecular diagnostics.[1−5] In particular, macrocyclic systems, for example, cryptands,[6,7] calix[*n*]arenes,[8−10] cavitands,[11−14] naphthotubes,[15−17] and cucurbit[*n*]urils[18,19] can strongly bind biorelevant analyte classes, such as metabolites, neurotransmitters, steroids, or metal cations in aqueous media. Unfortunately, macrocyclic hosts are in most cases composed of a fully covalently linked organic framework,[20−25] and thus, it can be challenging and time-consuming to tune their binding properties through the synthesis of new macrocyclic derivatives. Moreover, nearly all macrocyclic building blocks are structurally highly symmetric and consequently are rather unselective binders. In other words, they do not mimic the asymmetric and selective binding pocket of proteins.[26]

The installation of labile interaction motifs into supramolecular building blocks has become of recent interest as it allows for an adaptation of the molecular constitution in response to internal or external factors.[27−31] Indeed, the development and screening of some synthetic receptor families have been facilitated and accelerated in this way.[32−34] Nevertheless, it is unfortunately not obvious how to install dynamic covalent bonds into the framework of the aforementioned macrocyclic host classes.

For instance, while the propensity of cucurbit[*n*]uril (CB*n*) macrocycles to strongly bind a wide range of biorelevant organic compounds such as biogenic amines,[35] amino acids,[36] and steroids[37] in water has spurred the development of ingenious assays for monitoring biophysical and enzymatic processes,[38,39] successful applications of CB*n* chemosensing ensembles in biofluids, for example, for molecular diagnostic

Received: February 8, 2022
Published: July 18, 2022

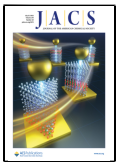

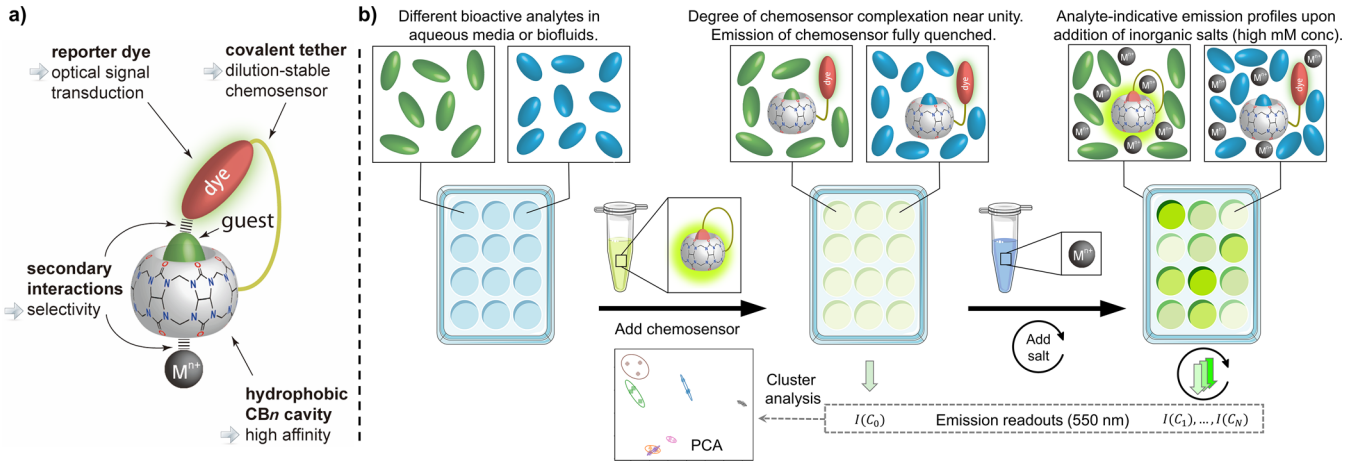

Figure 1. (a) Schematic representation of the herein introduced unimolecular CB*n*-based chemosensor that undergoes salt-induced adaptation and that can be used for the distinction of bioorganic analyte in aqueous media and biofluids. (b) Schematic principle of the salt-addition assay workflow that enables the distinction of biorelevant analytes through the salt-adaptive CB7-NBD chemosensor.

purposes, remain scarce.[40,41] There are two major obstacles that hamper the transfer of aqueous CB*n*-model systems to biofluids: (i) The analyte selectivity of CB*n* systems is relatively low compared to that of established biosensors, causing confounding cross-reactivity in complex media. (ii) As a consequence of their remarkable affinity to metal cations—for example, logK_a(CB7) = 3.41, 3.46, and 4.25 for Na^+, K^+, and Ca^{2+}, respectively[42]—CB*n*-guest complexation is also strongly subject to competitive binding by the salts occurring in biofluids.[43]

With synthetic advances for the preparation of functionalizable cucurbit[*n*]uril derivatives, new opportunities for the design of responsive CB*n* systems have emerged[44−46] with which ultra-strongly binding guests such as the drug amantadine can be detected in biofluids.[47] Nevertheless, sensing of less strongly binding metabolites or drugs has so far required the preparation and use of a library of differentially selective chemosensors in combination with multivariant data analysis.[9,48−50] In principle, it would be thus desirable to develop additional CB*n* derivatives and conjugates that display differential selectivity for particular biorelevant analytes of interest. However, despite many creative attempts yielding structurally fascinating CB*n* analogues such as chiral CB*n*, nor-seco-CB*n*, or acyclic CB*n*,[18,19,51,52] significant improvements of the native binding selectivity of CB*n* macrocycles have not been achieved yet.[53,54]

Herein, we introduce a new concept that turns the shortcomings of cucurbit[*n*]urils—their wide analyte-binding scope (→ low selectivity) and their propensity to bind metal cations (→ CB*n*·guest complex disintegration in saline media)—into distinctive and desirable features. Our report also demonstrates the future potential of sensing applications in biofluids with adaptive chemosensors.

RESULTS

Design of the Chemosensor. While adaptive chemosensors were expected to possess fascinating and desirable properties,[55] it was not obvious to us how to integrate dynamic covalent bonding motifs into the framework of macrocyclic synthetic binders such as cucurbit[*n*]urils. Herein, metal cation-host co-complexation is introduced for constructing an adaptive chemosensor.

The adverse effects of salts on the performance of non-covalently bound CB*n*⊃dye chemosensing ensembles are well known (see also Figure S1 for two instructive example dyes for CB7), which in the past prompted us and others to employ "minimal" buffers (e.g., 10 mM sodium phosphate) when setting up CB*n*-based assays.[56,57] We wondered if the sizeable affinity of CB*n* for metal cations can be exploited instead of mitigated for designing novel CB*n*-type chemosensors (Figure 1). In the ideal scenario, much more information about the molecular composition of a biorelevant medium can be harvested with a chemosensor whose analyte-binding properties and spectroscopic features are tunable through stepwise concentration increase in a single salt type, or through use of different salt types at a fixed concentration, or through a combination of both.

We reasoned that a covalently tethered reporter dye is needed to ensure the resistance of the chemosensing entity toward dilution and competitive salt binding, both of which are known to negatively impact the integrity of non-covalent CB*n*⊃dye chemosensing ensembles (Figure 1a). However, all the known CB*n*-binding reporter dyes[41,58] are likely not suitable for devising a unimolecular CB*n*-based chemosensor that is applicable for the detection and differentiation of bioorganic guests: First, when covalently tethering any of the known cationic and strongly binding reporter dyes such as berberine to CB7, one inevitably enhances their binding strength because the effective molarity is positive when using an appropriate tether length.[59] This results in a chemosensor that can detect only ultra-high-affinity synthetic guests concomitant with being unresponsive to weaker binding biorelevant compounds.[47] Second, a positively charged reporter dye will electrostatically repel metal cations and thus impede their binding to the carbonyl-fringed CB*n*-rim, thereby arriving at a salt-unresponsive chemosensor. In contrast, when grounding the unimolecular chemosensor design on inherently weakly binding and non-charged reporter dyes, a wide range of bioorganic guests will be targetable in aqueous media, and co-complexation of metal cations by the host framework will be exploitable for chemosensor adaptation and selectivity tuning (Figure 1b, top).

Selection of a Suitable Dye for Tethering to CB7. First, the available literature on environment-responsive non-charged fluorescent dyes was screened as they are expected to

https://doi.org/10.1021/jacs.2c01520
J. Am. Chem. Soc. 2022, 144, 13084−13095

provide an emission change upon inclusion into the hydrophobic CB7 cavity and at the same time likely tolerate co-binding of metal cations to CB7. Only dyes with suitable size dimensions for forming inclusion complexes with CB7 were considered. This removed all xanthene dyes from the candidate list. Furthermore, those dye candidates were excluded that have already been reported as CB7-binding dyes as their affinity would become too large upon their covalent tethering to the CB7 macrocycle. Finally, we funneled down on the small, non-charged, and highly solvent-polarity-responsive fluorescent reporter dye nitrobenzoxadiazole (NBD)[60] as a promising candidate for covalent tethering to CB7. Indeed, the hardly detectable spectral change of NBD upon addition of CB7 confirmed that CB7 and NBD do not form a binary inclusion complex in aqueous solution in the low micromolar concentration range (Figure S6), supporting our assumption that this polar and non-charged chromophore has a weak inherent affinity for CB7.

Synthesis of the CB7-NBD Chemosensor. In a first step, 4-chloro-7-nitrobenzofurazan (NBD-Cl) was conjugated to an azide-terminated tetraethylene glycol (TEG) chain. See Supporting Information for detailed synthetic procedures. Second, this NBD-TEG was covalently tethered to a propargyl-functionalized monosubstituted CB7 (prepared according to literature procedures[42]) via an azide-alkyne Huisgen cycloaddition reaction to obtain the CB7-NBD conjugate after purification by HPLC (Scheme 1).

Scheme 1. Preparation of CB7-NBD via an Azide-Alkyne Huisgen Cycloaddition

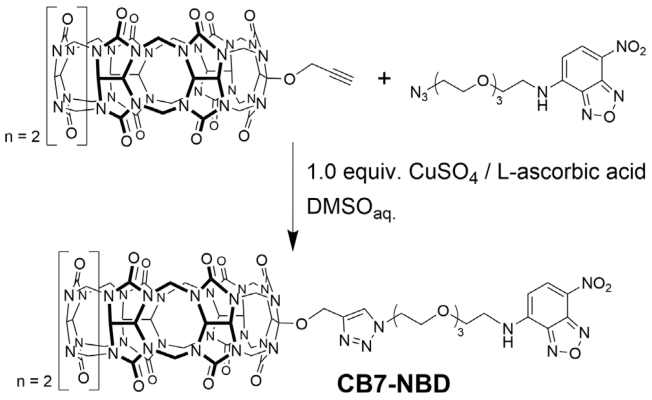

^{1}H NMR experiments were carried out to characterize the conformation of CB7-NBD in an aqueous solution. It was discovered that the NBD protons exhibit clear upfield shifts upon dye tethering to CB7 (Figure 2a,b). This observation is consistent with an inclusion of the NBD moiety in the CB7 cavity through the adoption of a folded, unimolecular complex structure. Noteworthily, the addition of salts markedly increased the solubility of CB7-NBD and the quality of the ^{1}H NMR spectrum, giving first evidence that the desired co-binding of metal cations to the chemosensor occurs.

Photophysical Features of CB7-NBD. As anticipated from the known photophysical properties of NBD dyes and self-inclusion complex formation, aqueous solutions of CB7-NBD are highly emissive (λ_{ex} = 475 nm, λ_{em} = 500−600 nm; see Figure 3a, bold black curve), whereas the corresponding NBD-TEG molecule on its own is very weakly fluorescent in aqueous solutions at the same concentration (Figure 3a, blue curve). Importantly, CB7-NBD responds uniquely toward the addition of inorganic salts as it features an emission enhancement and characteristic absorbance/emission maxima shifts which can be attributed to a strengthening of the unimolecular self-inclusion complex through cation co-binding (Figures S8−9 and Table S1). In contrast, all binary CB*n*⊃dye chemosensing ensembles that we are aware of undergo dye expulsion from the CB*n* cavity upon salt addition (Figure S10 showcases two examples).

Interaction of CB7-NBD with Bioorganic Analytes. When typical CB7-binding guests,[61,62] for example, cadaverine or amantadine, were added to an aqueous solution of CB7-NBD, inclusion complex formation with the analyte and concomitant displacement of the NBD fluorophore from the CB7 cavity occurred as was concluded from the characteristic ^{1}H NMR peak shifts (Figure 2c,d). Addition of excess analytes into a solution of CB7-NBD results in the NBD protons (marked with red and blue squares) undergoing significant downfield shifts ($\Delta\delta$ = 0.5 and 0.3 ppm, respectively). Note the slight but significant differences between the aromatic ^{1}H signals of NBD-TEG and the different CB7-NBD⊃guest complexes. These findings give the first indication that the NBD moiety of the guest-bound chemosensor is located in proximity to the CB*n* portals and may engage in additional interactions with the bound guest, as graphically depicted in Figure 1a. This mechanistic interpretation was further supported by the strong intensity decrease and slight bathochromic shift of the emission signal of CB7-NBD, indicating that the reporter dye was exposed to the polar solvent environment upon guest addition (Figure 3a). Likewise, guest addition to the chemosensor also caused a slight hypochromic and hyperchromic shift in the absorbance spectrum (Figure S11). Subtle but significant differences were discovered for the photophysical properties of the linker molecule NBD-TEG in comparison to the different CB7-NBD⊃guest complexes (Table S1).

Emission-based titration experiments were carried out to assess the binding strength of CB7-NBD with typical CB7-binding bioorganic guests (Figures S12−25 and Table 1). Pleasingly, it was observed that CB7-NBD shows only modestly reduced binding affinities compared to the parent molecule CB7, for example, logK_a = 7.0 *versus* 7.5 for PheGly[63] or 6.7 *versus* 7.4 for methyl viologen (M_2V)[64] complexation in deionized water. This supports that expulsion of the reporter dye NBD from the CB7 cavity causes only a low energetic cost instead of the previously observed strong guest-affinity reduction of strongly self-bonded CB7-BC.[47] Examples of typical analytes' binding affinities with CB7-NBD are listed in Table 1, which also provides a comparison between deionized water and 1X PBS (consisting of 137 mM NaCl, 2.7 mM KCl, 10 mM Na_2HPO_4, and 1.8 mM KH_2PO_4) as the media. Expectedly, logK_a values are markedly attenuated in the presence of the salts occurring in 1× PBS, yet they are still large compared to many other supramolecular hosts. Thus, the introduced chemosensor can be used to complex a wide range of bioorganic analytes in aqueous media.

At first sight, it may seem limiting with respect to sensing applications that CB7-NBD complexes many bioorganic analytes with similar affinity. It is now presented how this apparent shortcoming can be transformed into a useful feature by involving the unique response of CB7-NBD⊃guest complexes to the addition of salts.

https://doi.org/10.1021/jacs.2c01520
J. Am. Chem. Soc. 2022, 144, 13084−13095

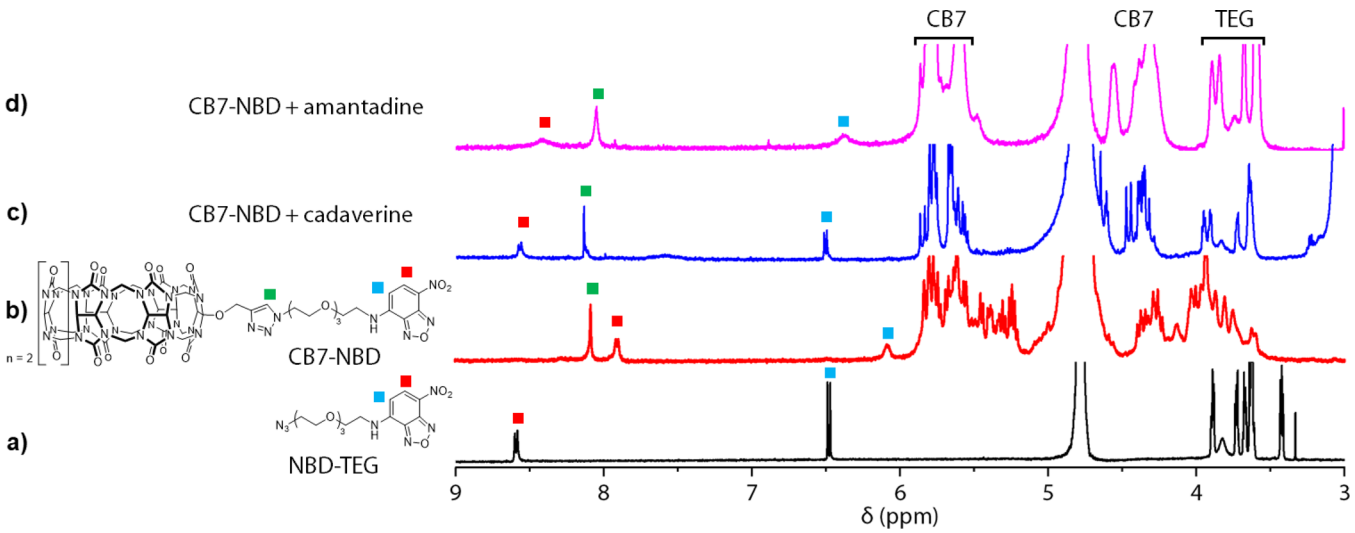

Figure 2. Overlay of ^{1}H NMR (500 MHz, D_2O) spectra of (a) NBD-TEG (black), (b) CB7-NBD (red), (c) CB7-NBD with an excess of cadaverine (blue), and (d) CB7-NBD with an excess of amantadine (pink). The appearance of the singlet peak at 8.04 ppm (marked with a green square) confirmed the triazole formation via click reaction.

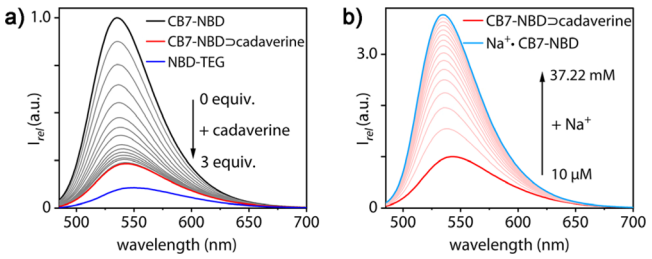

Figure 3. (a) Emission spectra (λ_{ex} = 475 nm) of CB7-NBD (1.0 μM) upon addition of cadaverine (from bold black curve to red curve) and NBD-N_3 (1.0 μM) (blue curve). (b) Representative emission-based titration of the CB7-NBD⊃cadaverine complex with $NaCl_{aq}$ (λ_{ex} = 475 nm).

Response of CB7-NBD⊃Guest Complexes to Salts. A unique behavior of CB7-NBD⊃guest complexes was observed when titrating their aqueous solutions with salts. For instance, Figure 3b shows the steep emission increase for CB7-NBD⊃cadaverine upon addition of $NaCl_{aq}$, indicating the expulsion of the dicationic cadaverine from the chemosensor cavity and the re-binding of the NBD moiety upon Na^+-co-complexation. The corresponding absorbance spectra corroborate this assumed binding model for cadaverine and other positively charged guests such as spermidine (Figure S11e,f). Conversely, $NaCl_{aq}$ addition to CB7-NBD inclusion complexes with the non-charged guest pinacol did not fully reverse the absorbance spectra to that of self-folded CB7-NBD (Figure S11c), which suggests that the guest remains engulfed in the host's cavity (and consequently, the NBD remains mostly outside the host's cavity), as depicted in Figure 1. Finally, CB7-NBD inclusion complexes with an ultra-high-affinity guest such as amantadine and 1-adamantanol were almost $NaCl_{aq}$-unresponsive. As will be discussed below, the interaction of salts with CB7-NBD does not merely cause only the competitive guest displacement from the CB7 cavity but induces the adaptation of different supramolecular structures (Scheme 2a) depending on the analyte type, salt type, and salt concentration present. In this respect, it is justifiable to term CB7-NBD a salt-adaptive chemosensor even though it lacks dynamic covalent bonding motifs.[65]

Table 1. Binding Affinities of CB7-NBD with Bioorganic Analytes from Fluorescence Titration Experiments in Aqueous Media[a]

analytes	logK_a (M^{-1})	
	H_2O	1× PBS
putrescine (Put)	5.2	≤3.0[b]
cadaverine (Cad)	7.0	4.0
spermidine (Spd)	6.3	3.3
spermine (Spm)	7.8	3.9
agmatine (Agm)	5.5	≤3.0[b]
tyramine (Tyr)	5.8	3.8
amantadine ($AdNH_2$)	≥8.0[b]	≥8.0[b]
L-phenylalanyl glycine (PheGly)	7.0	4.5
nandrolone (Nan)	[c]	4.2
methyl viologen (M_2V)	6.7	4.1
1-adamantanol (AdOH)	≥8.0[b]	[c]
pinacol	5.2	4.1
4-fluorophenethylamine (4F-PEA)	6.4	4.1
1,8-octanediyl-bis(methylimidazolium) (C_8mim)	≥8.0[b]	5.9

[a]10 μM NaCl was added to CB7-NBD (1 μM) for solubility reasons. The estimated error in logK_a is 0.2. 1× PBS consisting of 137 mM NaCl, 2.7 mM KCl, 10 mM Na_2HPO_4, and 1.8 mM KH_2PO_4. [b]Binding curves too flat (Put, Agm) or too steep (others); thus K_a determination was not attempted. [c]K_a determination not attempted due to slow equilibration.

Overall, it appears promising to devise a sensing assay where the analyte distinction is achieved by the differential emission responses of CB7-NBD analyte complexes to the addition of different concentrations and types of salts.

Microplate Assay Utilized for Analyte Distinction. The salt-based analyte distinction assay can be carried out in microwell plates with fluorescent plate readers, enabling array-based sensing strategies (see also Figure 1b). In this way, the emission responses of different CB7-NBD⊃analyte complexes to various salts were accessible in a convenient fashion in parallel experiments. The principle of our novel salt-addition assay for analyte distinction is schematically depicted in Scheme 2a. In the assay preparation step, CB7-NBD is added at a fixed sub-stoichiometric concentration to an aqueous

https://doi.org/10.1021/jacs.2c01520
J. Am. Chem. Soc. 2022, 144, 13084−13095

Scheme 2. (a) Schematic Representation of Salt-Induced Analyte Distinction by CB7-NBD.[a] b) Chemical Structures of the Tested Analytes.[b]

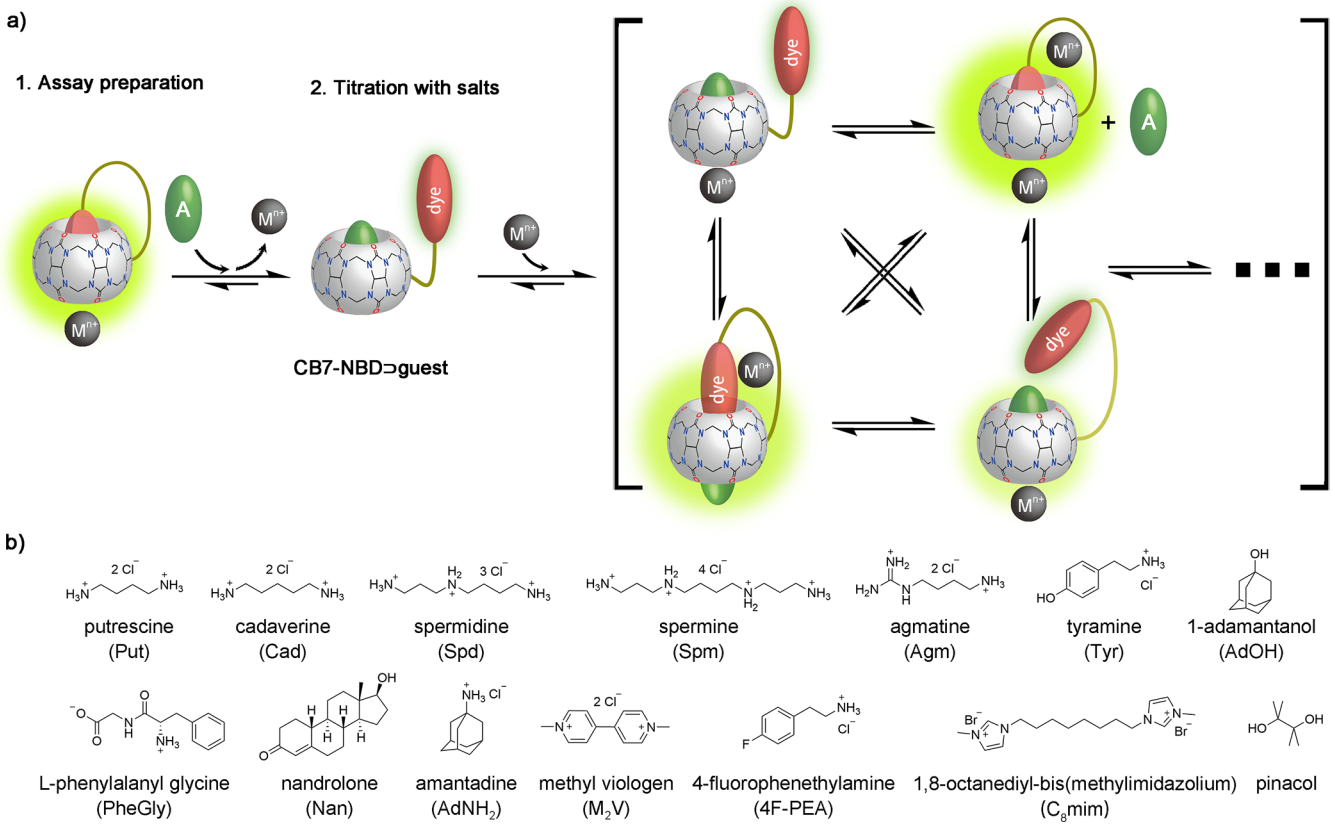

[a]Upon titrating with salts, some analytes are expelled from the chemosensor, while the dye moiety is rebound. Other CB7-NBD analyte complexes may adopt a different binding geometry but remain intact in the presence of salts. One or more equivalents of metal cations can be co-complexed as a function of salt concentration and salt type. These processes provide analyte-indicative information and enable their distinction. [b]All compounds are shown in their native charge state in water, pH 7.

solution of the analytes, thereby ensuring that a high degree of complexation of the chemosensor is reached relatively independent of the binding affinity of the guest. Inorganic salts, for example, alkaline chlorides, are then titrated stepwise into the assay mixture for which the emission intensity is recorded and plotted against the concentration of added salt.

The obtained salt concentration *versus* emission intensity plots are shown in Figures 4a and S26−53. The contrast to standard IDAs illustrates how our CB7-NBD-based salt-addition assay provides unique opportunities for analyte distinction in aqueous media. For instance, a much steeper emission increase was observed when titrating $NaCl_{aq}$ to a solution containing the CB7-NBD⊃biogenic amine complexes than the weak emission responses with the chemosensor in the presence of, for example, nandrolone (Nan), PheGly, or pinacol (Figure 4a). Moreover, CB7-NBD complexes with the ultra-high-affinity guests, adamantanol and amantadine, were almost unresponsive to $NaCl_{aq}$ addition and thus were directly identifiable compared to all other analytes tested. Thus, a subgrouping of guests can already be achieved by CB7-NBD through addition of a single salt.

Note also that control over the added salt concentration provides a facile path to harvest useful information for analyte distinction. For instance, while C_8mim, pinacol, and the control sample are difficult to distinguish when 300−500 mM NaCl was added, their distinction becomes apparent at >800 mM. In contrast, the distinction of the control sample from $AdNH_2$ and AdOH is possible when 300−500 mM NaCl is present but becomes infeasible when approaching 1000 mM NaCl. Furthermore, standard IDA-type non-covalent CB*n*⊃dye reporter pairs, for example, CB7⊃BC (Figure 4a,c, right side) and CB7⊃MDAP (Figure S55), or the cationic unimolecular chemosensor CB7-BC (Figure S57) were incapable of distinguishing the bioorganic analytes.

Additional and complementary information for the analyte distinction can be harvested when different salts are added, for example, NH_4^+ or alkaline (Li^+ to Cs^+) and earth alkaline metals (Mg^{2+} to Ba^{2+}). For instance, a much steeper emission increase was observed when titrating $LiCl_{aq}$ to a solution containing the CB7-NBD⊃spermidine complex than when adding $LiCl_{aq}$ to the CB7-NBD⊃spermine sample (Figure S28), while these two biogenic amines were less distinguishable by $NaCl_{aq}$ addition.

Data Analysis and Quantification of Analyte Salt-Response Differences. The chemosensor emission data gathered for each analyte sensing experiment result in additional data dimensions for each employed salt concentration and salt type. To arrive at visually easy-to-analyze graphs, the data dimensionality was reduced by principal component analysis (PCA), an unsupervised data analysis method that is widely employed in differential sensing studies.[49,67−69] First, PCA was performed solely on the

https://doi.org/10.1021/jacs.2c01520
J. Am. Chem. Soc. 2022, 144, 13084−13095

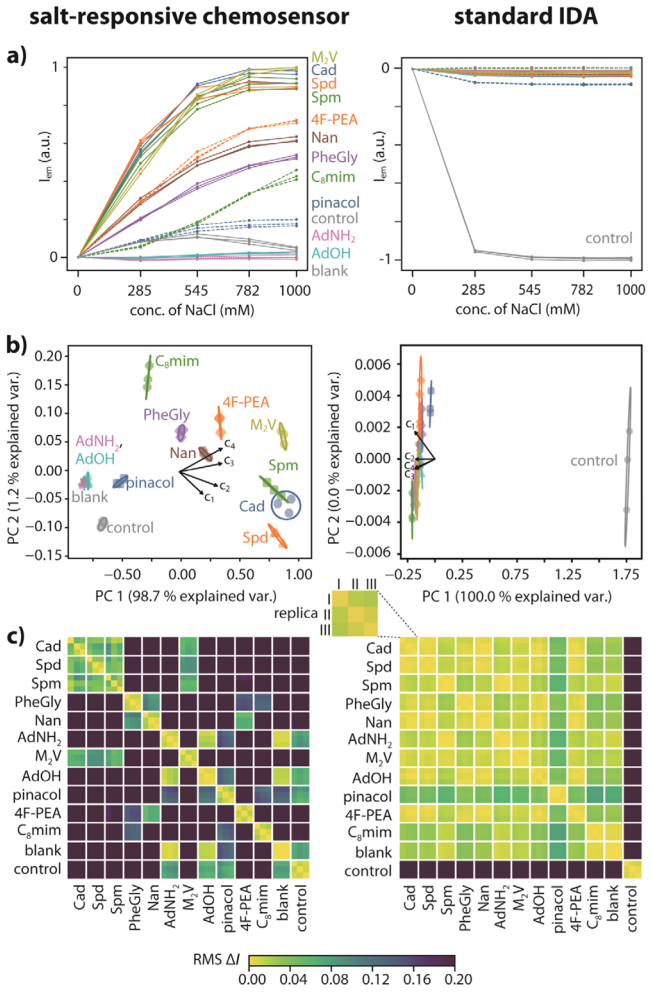

Figure 4. NaCl salt-addition response curves of the unimolecular chemosensor CB7-NBD, left, compared to a standard indicator displacement assay (IDA)[66] with a binary complex of CB7 and berberine chloride (BC), right. The assay was initiated by preparing a mixture of chemosensor (1.0 μM CB7-NBD or 1.0 μM CB7 + 1.2 μM BC) and 200 μM of the analyte in 10 mM phosphate buffer, pH 7.45. Note that the buffer contains 17 mM Na^+ cations. (a) Normalized plot of the emission intensity as a function of the concentration of added NaCl. Three replicas of the emission responses for each analyte-NaCl combination are shown. Control/blank: Experiments without CB7-binding analyte/without a chemosensor. (b) PCA biplot of the first two principal components of $I_{em}(c)$ after PCA with all analytes upon addition of NaCl and 95% confidence ellipses. The black *loading* vectors reflect the influence of each concentration on the first two principal components. Orthogonal vectors indicate uncorrelated information between the corresponding measurements, whereas parallel vectors indicate redundant information. Each arrow in the plot (c_1–c_4) corresponds to one concentration of NaCl (c_1 = 285 mM, c_2 = 545 mM, c_3 = 782 mM, and c_4 = 1000 mM). (c) Distances between any two replicas' emission responses. Distances were quantified through the normalized root mean squared deviation of the emission values at four concentrations of NaCl. The three replicas per analyte are depicted inside the blocks as smaller squares. The blocks correspond to different analytes and are separated by thick white lines. Yellow color marks small distances (curves are very similar); violet color marks larger distances (curves are more different).

single-salt NaCl-addition data with the data from all analytes together. We visualized the first two principal components of the I_{em} curves and the *loadings* of the four concentrations (Figure 4b). Distinct data clusters were observed for most analytes, substantiated by non-overlapping 95% confidence ellipses, which were computed from the replica measurements for each analyte. In summary, NaCl and other alkaline salts (Figures S28–35) performed excellently and enable the simultaneous distinction of many bioorganic analytes from each other. Titration with either KCl (Figure S31), NH_4NO_3 (Figure S41), or $NaNO_3$ (Figure S43) even sufficed to distinguish all analytes in this study without the need for an array-based setup. In contrast, the PCA graphs did not allow for analyte differentiation when the IDA-type chemosensing ensemble CB7⊃BC (Figure 4b) or other known CB*n*-based systems (Figures S55–58) were used instead of the salt-adaptive chemosensor CB7-NBD. This observation even holds true if the emission data curves for the control sample (= no CB7-binding analyte is present) and blank sample (= no chemosensor was added) were removed prior to the cluster analyses. While in this case, the PCA biplots expectedly showed clearer clustering of the analyte data points than in the presence of control and blank, the salt addition assay with CB7-NBD still offers a superior analyte distinction capability than the use of the standard IDA chemosensors (Figures S59–60). Second, if a single salt does not provide sufficient information to distinguish all pairs of analytes, additional information can be obtained from repeating the assay with further types of salts (Figures S26–53). For instance, while the data clusters for $AdNH_2$, AdOH, and the blank sample overlap for the NaCl addition data, $AdNH_2$ can be distinguished from AdOH by RbCl addition (Figure S32). Likewise, $La(NO_3)_3$ addition can be used to identify the blank sample (Figure S48).

Third, it is also possible to jointly process the data from all salt-addition measurements at once, that is, both the concentration dependence (herein $N_{\text{salt conc}} = 4$) and salt-type dependence (herein $N_{\text{salt types}} = 14$) and thus to involve $4 \times 14 = 56$ values for each analyte, which can further enhance the analyte distinction capabilities. Again, a common two-dimensional PCA can be used for this analysis (Figure S54), but we suggest involving a three-dimensional PCA or other machine learning techniques to better reflect and leverage the additional amount of information available (see the Supporting Information for more details).

The opportunity to obtain additional data by salt addition to a single chemosensor is a major asset of our assay format compared to previous receptor-library-based approaches, for which it is necessary to synthesize many artificial binders. However, we found that it was not required to employ many different salts for our analyte test set—the data obtained from four concentrations of 1–2 different salt types (mostly alkaline salts) appeared generally sufficient for analyte distinction. Table S2 lays out which pairs of analytes can be separated by which salts. It is worth noting that a growing number of salt types, analogue to using a growing number of IDA receptors, statistically increases the chance of false discoveries of differences between analytes (multiple comparisons problem). If necessary, this can be addressed with Bonferroni correction.[70]

In order to summarize the difference between the salt responses of any pair of specimens a and b in a single, intuitive quantity, the root mean squared deviation of the salt-induced emission responses I_{em} was calculated for each salt (offset-corrected $(I_{em}(c) \rightarrow I_{em}(c) - I_{em}(c = 0))$ and normalized $(I_{em}(c) \rightarrow I_{em}(c)/\max(|I_{em}(\text{all concentrations and analytes})|)$:

https://doi.org/10.1021/jacs.2c01520
J. Am. Chem. Soc. 2022, 144, 13084–13095

$$\Delta(I_a, I_b) = \sqrt{\frac{\sum_c (I_a(c) - I_b(c))^2}{N_{conc}}} \quad (1)$$

where c stands for the salt concentration and, again, $N_{salt\ conc}$ for the number of different salt concentrations used in the assay.

The corresponding plots that depict the pairwise distance $\Delta(I_a, I_b)$ between any two replicas/samples are presented in Figure 4c. It can be seen that except for the ultra-high-affinity guests, adamantanol and amantadine, whose CB7-NBD complexes are essentially salt-unresponsive, it is generally feasible to pairwisely distinguish two analytes from each other when selecting an appropriate salt as a titrant.

Differential sensing of analyte mixtures was also investigated using the salt-addition approach. For demonstration purposes, mixtures of spermine and nandrolone were utilized and found to be clearly distinguishable from each other, for instance, through the titration with $NaCl_{aq}$, see Figures S61−62.

Differentiation of Biogenic Amines by Salt-Addition Assays. In order to elucidate the future prospects of salt-adaptive chemosensors, we attempted the distinction of the most important biogenic amines, that is, putrescine, cadaverine, agmatine, tyramine, spermidine, and spermine, which are all polycationic, see also Scheme 2b for their chemical structures and Table S3 for their physiological occurrences in different biofluids. Figures S63−68 present the array-based emission data for salt addition to solutions containing biogenic amines (500 μM) and CB7-NBD (1 μM) in 10 mM phosphate buffer, pH 7.45. Generally, the salt-adaptive CB7-NBD chemosensor appears capable of distinguishing also these structurally similar and thus challenging analytes from each other. Similar observations were made for the salt-response data obtained at 200 μM concentration of biogenic amines, suggesting that the assay is not adversely disturbed by concentration differences if the analyte occurs at concentration excess compared to the chemosensor such that a high degree of chemosensor complexation is ensured when initiating the salt-addition assay (Figures S69−76). Salt-addition assays were also carried out at 10 times lower concentration (20 μM) of biogenic amines in the presence of 0.1 or 0.25 μM of CB7-NBD (Figures S77−84). Again, all analytes were clearly distinguishable from each other in both corresponding PCA and distance plots.

Application of CB7-NBD to Human Biofluids. Having established the stability of CB7-NBD and its utility for analyte differentiation in 10 mM phosphate buffer, we wondered if the chemosensor can also be applied to biofluids. This is a scenario where most supramolecular chemosensors, particularly also contemporary CB*n*-based systems, lose any prospect due to their disintegration or unselective binding properties. Thus, the performance of the salt-addition assay with CB7-NBD was first tested in analyte-spiked biofluids such as human urine and deproteinized human serum (Figure 5a,b) as well as in artificial saliva and artificial synthetic urine (surine), see Figures S85−90.

It is very encouraging to see that our chemosensor in combination with the salt-addition assay is well suited for distinguishing all spiked biofluid specimens from each other. The only difficulty arose again for the distinction of the ultra-high-affinity guests, for which CB7-BC can be a more suitable chemosensor choice.[47]

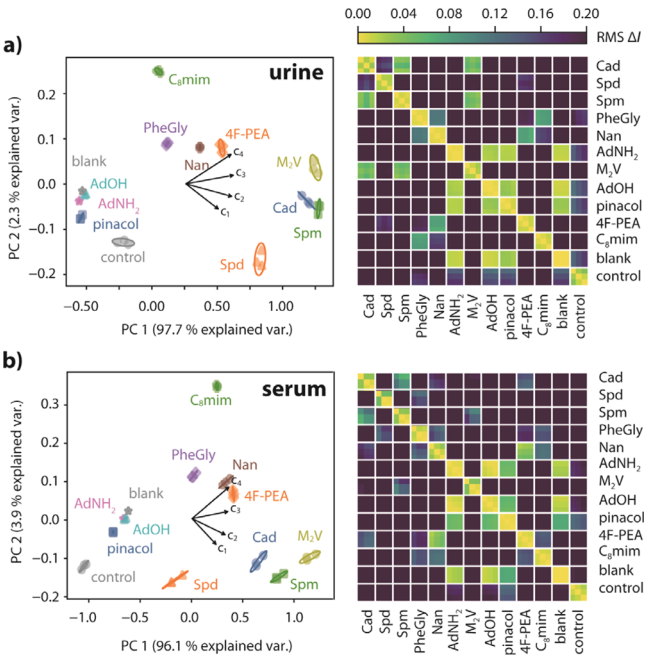

Figure 5. PCA biplots with 95% confidence ellipses resulting from the emission intensity at 550 nm (λ_{ex} = 475 nm) as a function of the concentration of added NaCl with 1 μM CB7-NBD in (a) human urine spiked with 200 μM analytes and (b) diluted human deproteinized serum spiked with 200 μM analytes. The corresponding colorimetric plots for differences in emission response between pairwise replicas/samples were presented on the right side.

Finally, we also evaluated if different non-spiked urine samples from healthy volunteer donors can be differentiated from each other. This was indeed the case, both for the parent urine samples (which also differed in their background emission) and for pre-diluted urine samples that were adjusted to a similar or nearly identical background emission prior to chemosensor and salt addition (Figures S91−93). On the one hand, such matrix effects are not desirable for specific analyte sensing. On the other hand, we intend to apply our salt-addition chemosensor protocol to urine samples from healthy donors *versus* that of diseased patients to develop a method for subgrouping of patient samples. In this scenario, a composite response caused by the interplay of many analytes in the matrix might not be a disadvantage. Note again that the information content available can be easily increased by the use of additional salts (see Supporting Information, Figures S85−88 show this for spiked saliva samples that were analyzed by CB7-NBD through the addition of NaCl and CsCl) or other types of chemosensors.

Characterization of the Binding Geometries by Ion Mobility Experiments and DFT Calculation. Encouraged by the promising analyte distinction capabilities of CB7-NBD, we aimed to uncover a molecular picture of its binding modes. Thus, ion mobility experiments were combined with DFT calculations to unravel the conformations of analyte-bound and unbound CB7-NBD chemosensor. Further, we hoped to identify differences to the complex geometries of literature-known CB*n*-guest complexes.[71,72]

Figure 6a displays a representative structure of a Na^+·CB7-NBD complex that was geometry-optimized by dispersion-corrected DFT calculations, see Supporting Information for details. The energetically lowest conformer (out of 10

https://doi.org/10.1021/jacs.2c01520
J. Am. Chem. Soc. 2022, 144, 13084−13095

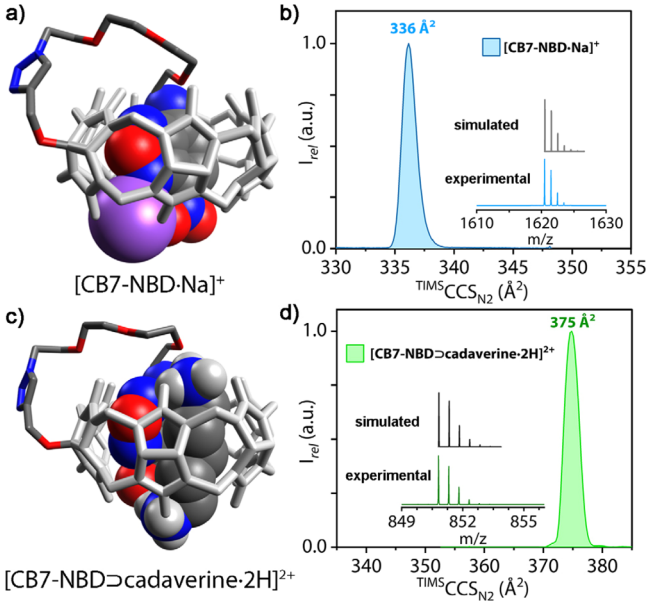

Figure 6. Left: Structures of (a) $[CB7\text{-}NBD{\cdot}Na]^+$ and (c) $[CB7\text{-}NBD{\supset}cadaverine{\cdot}2H]^{2+}$ obtained at the DFT level (BP86/disp3-bj/def2-SV(P)). The guest molecules and the NBD unit inside the cavity are depicted with van der Waals spheres. Hydrogen atoms are not shown for clarity, *except for the two protonated amino groups of cadaverine.* The CB7 unit is shown in light gray. Atoms colored in blue, red, and gray refer to nitrogen, oxygen, and carbon atoms, respectively. The sodium cation is shown in purple. Right: Mass spectra and ion mobilograms of (b) $[CB7\text{-}NBD{\cdot}Na]^+$ and (d) $[CB7\text{-}NBD{\supset}cadaverine{\cdot}2H]^{2+}$.

investigated conformers) showed the expected inclusion structure of the CB7-NBD linker and the bonding interaction of Na^+ with −CO− groups of CB7 and the $-NO_2$ moiety of NBD with Na−O distances of 2.34 and 2.23 Å, respectively. The structure and Mulliken charge distributions were then used to calculate collision cross sections (CCSs) based on the trajectory method (TM),[73] see the Supporting Information. Direct experimental support for this predicted conformer structure was obtained from ion mobility experiments, where only one conformer of the $Na^+{\cdot}$CB7-NBD complex (Figure 6b) was observed in the gas phase. Pleasingly, a good match between the experimentally determined CCSs and the calculated CCSs was found (Figure 6b and Table S4). For comparison, hypothetical unfolded structures with an external NBD moiety were calculated. These structures exhibit considerably higher DFT energies and also much larger CCS values that are not in agreement with the experimentally obtained ion mobility cross sections (Figure S96a and Table S4). A similar combined experimental-computational strategy was pursued for characterizing three representative CB7-NBD⊃guest complexes, namely, with cadaverine, adamantanol, and amantadine as guests.

For the double protonated $[CB7\text{-}NBD{\supset}cadaverine{\cdot}2H]^{2+}$ complex, DFT calculations suggest that a highly unusual dual CB7-inclusion complex is formed when the guest occurs in its native double protonated state (Figure 6c). The available experimental evidence, that is, the measured CCS is in good agreement with the computed complex structure (Figure 6d), whereas the most "intuitive" simple cadaverine inclusion complex with a dangling NBD chromophore can be excluded both from its computed conformation energy and from the discrepancy to the measured CCS value. Instead, both the NBD chromophore and cadaverine·$2H^+$ reside side-by-side, which provides a rationale why distinct photophysical properties have been observed for this system also in solution (see above). To the best of our knowledge, these computational and experimental results are the clearest indications known so far that CB7 can form ternary complexes akin to the well-known dual guest complexation mode of CB8. In contrast, for the monoprotonated $[CB7\text{-}NBD{\supset}cadaverine{\cdot}H]^+$ complex, an entirely different, exclusion-type structure was predicted by DFT calculations as the energetically lowest conformer which corroborated with ion mobility experiments (Figure S101b and Table S4). Likewise, calculations and ion mobility experiments for the $[CB7\text{-}NBD{\cdot}Na{\supset}adamantanol]^+$and the $[CB7\text{-}NBD{\cdot}Na{\supset}amantadine{\cdot}H]^{2+}$ complex also suggest an exclusion-type geometry with NBD remaining engulfed in the host's cavity (Figures S103a and S105a, Table S4). Conversely, in aqueous solution, it is much more likely that the AdOH and $AdNH_2$ guests are bound inside the CB7 cavity, while the NBD chromophore is exposed to the solvent, see again the ^1H NMR data in Figure 2. In the gas phase, the molecules are in an isolated state, that is, devoid of solvent molecules. This might lead to different topologies in the gas-phase compared to their solution-phase structures.

DISCUSSION

Two complementary approaches are typically pursued to improve the applicability of synthetic binders for analyte detection in complex mixtures: (i) Additional recognition motifs ("lock-and-key elements") are introduced into the receptor design,[74,75] which in turn increases the synthetic requirements. Unfortunately, this strategy appears not to be readily generalizable to many synthetic receptor classes. (ii) Differential sensing routines have become popular as an alternative strategy to circumvent the need for selectively binding synthetic receptors and some notable examples for drug sensing in (analyte spiked) buffers or biofluids have appeared.[48,49,76,77] Nevertheless, prevailing disadvantages of the array-based sensing approach are the need for synthesizing a library of differentially selective receptors and a hampered analyte identification when its concentration is unknown. More recently, a "dimer-dye disassembly assay" calix[*n*]arene-type receptor[78] and the "imprint-and-report"[68] strategy for dynamic combinatorial libraries were introduced that alleviate much of the synthetic burden. However, it is not obvious if those principles can be applied to cucurbit[*n*]uril-based sensing systems.

We devised a unimolecular CB7-based chemosensor that not only is dilution-stable and applicable in biofluids (other than parent CB*n* chemosensing ensembles) but that nevertheless maintains the high affinity and broad analyte-binding scope typical of cucurbit[*n*]urils. The selectivity of the herein introduced unimolecular CB7-NBD host-dye conjugate can be readily modulated through the addition of metal cations (salts), which in combination with the tethered non-charged reporter dye can engage in secondary interactions with the cavity-bound analyte. In-depth experimental measurements such as ^1H NMR, photophysics, ion mobility measurements, and theoretical investigations (DFT calculations) provided ample evidence for the proposed binding model. Our design principle provides the first practically feasible approach for modifying the native binding selectivity of CB*n* by the facile addition of different types of salts. Consequently, the synthetic

https://doi.org/10.1021/jacs.2c01520
J. Am. Chem. Soc. 2022, 144, 13084−13095

effort is kept low as one CB*n*-dye conjugate suffices to distinguish several analytes from each other. Furthermore, the herein proposed array-based sensing concept solves some of the shortcomings of contemporary differential sensing approaches. First, by using only a substoichiometric amount of chemosensor (Figure 1b), our assay format is not only more economical but importantly also reduces the impact of complicating degree-of-complexation differences between different analytes. In our case, a high degree of chemosensor complexation was reached for all tested analytes.

The most important information that is harvested in our assay format is the unique response of the chemosensor analyte complexes to the addition of different concentrations or types of salts. In contrast, established differential sensing assays typically probe characteristic differences in the degree of receptor complexation, which is not only subject to the type of analyte but also to its concentration, such that analyte identification can be hampered if the concentrations are unknown.

Presently, it appears unlikely that the ultra-high selectivity biosensors, for example, antibodies and aptamers, can be reached with current CB*n*-based chemosensor designs. Yet, our introduced CB7-NBD salt-addition assay already achieved the distinction of biogenic amines at a 20 μM concentration level that comes close to the physiological range in urine and saliva (Table S3). However, microplate-based experiments did not yield reliably distinct curves for biogenic amines at 1.0 μM concentration in buffer. Thus, further design improvements are needed for the physiological detection of biogenic amines in blood serum. Nevertheless, the herein described measurement routines can be readily performed in a standard fluorescent-based microplate reader that is equipped with an injector for salt addition within a few minutes—the equilibration time of CB*n*-guest complexation is extremely fast[79,80] and no additional washing steps are needed. Moreover, the data analysis can be carried out within a few seconds through automated software scripts. Thus, the evaluation of CB7-NBD for the analysis of urine or saliva in a clinical setting may be already considered, for example, to attempt a subgrouping of biofluid samples from patients, for example, into "healthy" and "diseased", for example, through pattern recognition and machine learning protocols. In this case, it may be necessary to account for the sample-inherent salt concentration, which can be easily estimated by ion conductivity measurements.[81] For biofluids with relatively narrowly distributed sample-to-sample salt concentration differences, for example, serum, the salt-addition assay is likely not significantly affected by matrix-to-matrix differences. Finally, it is worth pointing out again that even the titration with *one* type of salt (e.g., KCl) sufficed to clearly distinguish all 14 mixtures of bioorganic analytes with CB7-NBD from each other. Thus, our proposed assay does not need to be carried out in an array-based format, but can be if desired.

CONCLUSIONS

It was shown that the salt-adaptive behavior of cucurbit[7]uril-type supramolecular host-guest complexes can be exploited for differential analyte sensing. This novel unimolecular chemosensor sidesteps the limiting low binding selectivity of cucurbit[*n*]urils and the need to synthesize a library of differentially selective receptors by offering an information-rich data output that can be used for differential sensing analysis and machine learning. The presented chemosensor can be used for the sensing of bioorganic analytes in complex media such as blood serum, urine, and saliva. Moreover, this study identified a highly unusual ternary binding geometry for CB7 complexes.

The herein demonstrated salt-addition assay may be transferable to other macrocyclic synthetic receptors that possess an inherent affinity for inorganic anions or cations and engulf their bioorganic analytes in a shielded binding pocket.

ASSOCIATED CONTENT

Supporting Information

The Supporting Information is available free of charge at https://pubs.acs.org/doi/10.1021/jacs.2c01520.

Experimental details, synthetic procedures and characterizations of CB7-NBD, absorption and emission spectra, salt-addition assays, titration plots of binding affinities, PCA biplots and deviation heatmaps, mass spectra and ion mobilograms, and geometry-optimized molecular structures (PDF)

AUTHOR INFORMATION

Corresponding Authors

Thomas Jochmann − *Department of Computer Science and Automation, Technische Universität Ilmenau, Ilmenau 98693, Germany;* orcid.org/0000-0002-3564-4127; Email: thomas.jochmann@tu-ilmenau.de

Manfred M. Kappes − *Institute of Nanotechnology (INT), Karlsruhe Institute of Technology (KIT), Eggenstein-Leopoldshafen 76344, Germany; Institute of Physical Chemistry (IPC), Karlsruhe Institute of Technology (KIT), Karlsruhe 76131, Germany;* orcid.org/0000-0002-1199-1730; Email: manfred.kappes@kit.edu

Frank Biedermann − *Institute of Nanotechnology (INT), Karlsruhe Institute of Technology (KIT), Eggenstein-Leopoldshafen 76344, Germany;* orcid.org/0000-0002-1077-6529; Email: frank.biedermann@kit.edu

Authors

Changming Hu − *Institute of Nanotechnology (INT), Karlsruhe Institute of Technology (KIT), Eggenstein-Leopoldshafen 76344, Germany;* orcid.org/0000-0002-1220-003X

Papri Chakraborty − *Institute of Nanotechnology (INT), Karlsruhe Institute of Technology (KIT), Eggenstein-Leopoldshafen 76344, Germany; Institute of Physical Chemistry (IPC), Karlsruhe Institute of Technology (KIT), Karlsruhe 76131, Germany;* orcid.org/0000-0002-1353-7734

Marco Neumaier − *Institute of Nanotechnology (INT), Karlsruhe Institute of Technology (KIT), Eggenstein-Leopoldshafen 76344, Germany;* orcid.org/0000-0002-3810-3377

Pavel A. Levkin − *Institute of Biological and Chemical Systems − Functional Molecular Systems (IBCS-FMS), Karlsruhe Institute of Technology (KIT), Eggenstein-Leopoldshafen 76344, Germany*

Complete contact information is available at: https://pubs.acs.org/10.1021/jacs.2c01520

Author Contributions

The manuscript was written through the contributions of all authors. All authors have given approval to the final version of the manuscript. C.H. and T.J. share the first authorship.

Notes

The authors declare no competing financial interest.

The dataset and the data analysis source code are openly available in the Zenodo repository, https://doi.org/10.5281/zenodo.6451668.

■ ACKNOWLEDGMENTS

C.H. acknowledges the China Scholarship Council (No.201806920036). F.B. acknowledges the Emmy Noether program and the SPP 1807 of the Deutsche Forschungsgemeinschaft (BI-1805/2-1). P.C, M.N, and M.M.K. acknowledge KNMF and KIT for the mass spectrometry facility. P.C. acknowledges Alexander von Humboldt foundation for her postdoctoral research fellowship. T.J. acknowledges support from the Free State of Thuringia within the thurAI project (2021 FGI 0008). P.A.L. acknowledges the DFG (Heisenberg-professur Projektnummer: 406232485, LE 2936/9-1). Figure 1 includes modified lab equipment artworks from smart.servier.com (CC BY 3.0).

■ REFERENCES

(1) Escobar, L.; Ballester, P. Molecular Recognition in Water Using Macrocyclic Synthetic Receptors. *Chem. Rev.* **2021**, *121*, 2445−2514.

(2) Hargrove, A. E.; Nieto, S.; Zhang, T.; Sessler, J. L.; Anslyn, E. V. Artificial Receptors for the Recognition of Phosphorylated Molecules. *Chem. Rev.* **2011**, *111*, 6603−6782.

(3) You, L.; Zha, D.; Anslyn, E. V. Recent Advances in Supramolecular Analytical Chemistry Using Optical Sensing. *Chem. Rev.* **2015**, *115*, 7840−7892.

(4) Bell, T. W.; Hext, N. M. Supramolecular optical chemosensors for organic analytes. *Chem. Soc. Rev.* **2004**, *33*, 589−598.

(5) Grimm, L. M.; Sinn, S.; Krstić, M.; D'Este, E.; Sonntag, I.; Prasetyanto, E. A.; Kuner, T.; Wenzel, W.; De Cola, L.; Biedermann, F. Fluorescent Nanozeolite Receptors for the Highly Selective and Sensitive Detection of Neurotransmitters in Water and Biofluids. *Adv. Mater.* **2021**, *33*, No. 2104614.

(6) Zhang, M.; Yan, X.; Huang, F.; Niu, Z.; Gibson, H. W. Stimuli-Responsive Host−Guest Systems Based on the Recognition of Cryptands by Organic Guests. *Acc. Chem. Res.* **2014**, *47*, 1995−2005.

(7) Lehn, J. M.; Sauvage, J. P.; Cryptates, X. V. I. [2]-Cryptates. Stability and selectivity of alkali and alkaline-earth macrobicyclic complexes. *J. Am. Chem. Soc.* **1975**, *97*, 6700−6707.

(8) Zhang, Z.; Yue, Y.-X.; Xu, L.; Wang, Y.; Geng, W.-C.; Li, J.-J.; Kong, X.-L.; Zhao, X.; Zheng, Y.; Zhao, Y.; Shi, L.; Guo, D.-S.; Liu, Y. Macrocyclic-Amphiphile-Based Self-Assembled Nanoparticles for Ratiometric Delivery of Therapeutic Combinations to Tumors. *Adv. Mater.* **2021**, *33*, No. 2007719.

(9) Beatty, M. A.; Selinger, A. J.; Li, Y.; Hof, F. Parallel Synthesis and Screening of Supramolecular Chemosensors That Achieve Fluorescent Turn-on Detection of Drugs in Saliva. *J. Am. Chem. Soc.* **2019**, *141*, 16763−16771.

(10) Selinger, A. J.; Cavallin, N. A.; Yanai, A.; Birol, I.; Hof, F. Template-Directed Synthesis of Bivalent, Broad-Spectrum Hosts for Neuromuscular Blocking Agents**. *Angew. Chem., Int. Ed.* **2022**, *61*, No. e202113235.

(11) Murray, J.; Kim, K.; Ogoshi, T.; Yao, W.; Gibb, B. C. The aqueous supramolecular chemistry of cucurbit[n]urils, pillar[n]arenes and deep-cavity cavitands. *Chem. Soc. Rev.* **2017**, *46*, 2479−2496.

(12) Biros, S. M.; Rebek, J. J. Structure and binding properties of water-soluble cavitands and capsules. *Chem. Soc. Rev.* **2007**, *36*, 93−104.

(13) Yang, J.-M.; Chen, Y.-Q.; Yu, Y.; Ballester, P.; Rebek, J. Rigidified Cavitand Hosts in Water: Bent Guests, Shape Selectivity, and Encapsulation. *J. Am. Chem. Soc.* **2021**, *143*, 19517−19524.

(14) Soncini, P.; Bonsignore, S.; Dalcanale, E.; Ugozzoli, F. Cavitands as versatile molecular receptors. *J. Org. Chem.* **1992**, *57*, 4608−4612.

(15) Yang, L.-P.; Wang, X.; Yao, H.; Jiang, W. Naphthotubes: Macrocyclic Hosts with a Biomimetic Cavity Feature. *Acc. Chem. Res.* **2020**, *53*, 198−208.

(16) Huang, X.; Wang, X.; Quan, M.; Yao, H.; Ke, H.; Jiang, W. Biomimetic Recognition and Optical Sensing of Carboxylic Acids in Water by Using a Buried Salt Bridge and the Hydrophobic Effect. *Angew. Chem., Int. Ed.* **2021**, *60*, 1929−1935.

(17) Jia, F.; Schröder, H. V.; Yang, L.-P.; von Essen, C.; Sobottka, S.; Sarkar, B.; Rissanen, K.; Jiang, W.; Schalley, C. A. Redox-Responsive Host−Guest Chemistry of a Flexible Cage with Naphthalene Walls. *J. Am. Chem. Soc.* **2020**, *142*, 3306−3310.

(18) Minami, T.; Esipenko, N. A.; Zhang, B.; Kozelkova, M. E.; Isaacs, L.; Nishiyabu, R.; Kubo, Y.; Anzenbacher, P. Supramolecular Sensor for Cancer-Associated Nitrosamines. *J. Am. Chem. Soc.* **2012**, *134*, 20021−20024.

(19) Prabodh, A.; Bauer, D.; Kubik, S.; Rebmann, P.; Klärner, F. G.; Schrader, T.; Delarue Bizzini, L.; Mayor, M.; Biedermann, F. Chirality sensing of terpenes, steroids, amino acids, peptides and drugs with acyclic cucurbit[n]urils and molecular tweezers. *Chem. Commun.* **2020**, *56*, 4652−4655.

(20) Pedersen, C. J. The Discovery of Crown Ethers. *Science* **1988**, *241*, 536−540.

(21) Cram, D. J. The Design of Molecular Hosts, Guests, and Their Complexes. *Science* **1988**, *240*, 760−767.

(22) Freeman, W. A.; Mock, W. L.; Shih, N. Y. Cucurbituril. *J. Am. Chem. Soc.* **1981**, *103*, 7367−7368.

(23) Crini, G. Review: A History of Cyclodextrins. *Chem. Rev.* **2014**, *114*, 10940−10975.

(24) Kappe, T. The early history of calixarene chemistry. *J. Inclusion Phenom. Mol. Recognit. Chem.* **1994**, *19*, 3−15.

(25) Ogoshi, T.; Kanai, S.; Fujinami, S.; Yamagishi, T.-A.; Nakamoto, Y. para-Bridged Symmetrical Pillar[5]arenes: Their Lewis Acid Catalyzed Synthesis and Host−Guest Property. *J. Am. Chem. Soc.* **2008**, *130*, 5022−5023.

(26) Stank, A.; Kokh, D. B.; Fuller, J. C.; Wade, R. C. Protein Binding Pocket Dynamics. *Acc. Chem. Res.* **2016**, *49*, 809−815.

(27) Grote, Z.; Scopelliti, R.; Severin, K. Adaptive Behavior of Dynamic Combinatorial Libraries Generated by Assembly of Different Building Blocks. *Angew. Chem., Int. Ed.* **2003**, *42*, 3821−3825.

(28) Giuseppone, N.; Schmitt, J.-L.; Lehn, J.-M. Driven Evolution of a Constitutional Dynamic Library of Molecular Helices Toward the Selective Generation of [2 × 2] Gridlike Arrays under the Pressure of Metal Ion Coordination. *J. Am. Chem. Soc.* **2006**, *128*, 16748−16763.

(29) Ruff, Y.; Garavini, V.; Giuseppone, N. Reversible Native Chemical Ligation: A Facile Access to Dynamic Covalent Peptides. *J. Am. Chem. Soc.* **2014**, *136*, 6333−6339.

(30) Vantomme, G.; Jiang, S.; Lehn, J.-M. Adaptation in Constitutional Dynamic Libraries and Networks, Switching between Orthogonal Metalloselection and Photoselection Processes. *J. Am. Chem. Soc.* **2014**, *136*, 9509−9518.

(31) Black, S. P.; Stefankiewicz, A. R.; Smulders, M. M. J.; Sattler, D.; Schalley, C. A.; Nitschke, J. R.; Sanders, J. K. M. Generation of a Dynamic System of Three-Dimensional Tetrahedral Polycatenanes. *Angew. Chem., Int. Ed.* **2013**, *52*, 5749−5752.

(32) Otto, S.; Severin, K., Dynamic Combinatorial Libraries for the Development of Synthetic Receptors and Sensors. In *Creative Chemical Sensor Systems*, Schrader, T., Ed.; Springer Berlin Heidelberg: Berlin, Heidelberg, 2007; 267−288.

(33) de Bruin, B.; Hauwert, P.; Reek, J. N. H. Dynamic Combinatorial Chemistry: The Unexpected Choice of Receptors by Guest Molecules. *Angew. Chem., Int. Ed.* **2006**, *45*, 2660−2663.

(34) Rauschenberg, M.; Bomke, S.; Karst, U.; Ravoo, B. J. Dynamic Peptides as Biomimetic Carbohydrate Receptors. *Angew. Chem., Int. Ed.* **2010**, *49*, 7340−7345.

(35) Isobe, H.; Tomita, N.; Lee, J. W.; Kim, H.-J.; Kim, K.; Nakamura, E. Ternary Complexes Between DNA, Polyamine, and Cucurbituril: A Modular Approach to DNA-Binding Molecules. *Angew. Chem., Int. Ed.* **2000**, *39*, 4257−4260.

(36) Wang, B.; Han, J.; Bojanowski, N. M.; Bender, M.; Ma, C.; Seehafer, K.; Herrmann, A.; Bunz, U. H. F. An Optimized Sensor Array Identifies All Natural Amino Acids. *ACS Sens.* **2018**, *3*, 1562−1568.
(37) Lazar, A. I.; Biedermann, F.; Mustafina, K. R.; Assaf, K. I.; Hennig, A.; Nau, W. M. Nanomolar Binding of Steroids to Cucurbit[n]urils: Selectivity and Applications. *J. Am. Chem. Soc.* **2016**, *138*, 13022−13029.
(38) Nau, W. M.; Ghale, G.; Hennig, A.; Bakirci, H.; Bailey, D. M. Substrate-Selective Supramolecular Tandem Assays: Monitoring Enzyme Inhibition of Arginase and Diamine Oxidase by Fluorescent Dye Displacement from Calixarene and Cucurbituril Macrocycles. *J. Am. Chem. Soc.* **2009**, *131*, 11558−11570.
(39) Hennig, A.; Bakirci, H.; Nau, W. M. Label-free continuous enzyme assays with macrocycle-fluorescent dye complexes. *Nat. Methods* **2007**, *4*, 629−632.
(40) Krämer, J.; Kang, R.; Grimm, L. M.; De Cola, L.; Picchetti, P.; Biedermann, F. Molecular Probes, Chemosensors, and Nanosensors for Optical Detection of Biorelevant Molecules and Ions in Aqueous Media and Biofluids. *Chem. Rev.* **2022**, *122*, 3459−3636.
(41) Sinn, S.; Biedermann, F. Chemical Sensors Based on Cucurbit[n]uril Macrocycles. *Isr. J. Chem.* **2018**, *58*, 357−412.
(42) Zhang, S.; Assaf, K. I.; Huang, C.; Hennig, A.; Nau, W. M. Ratiometric DNA sensing with a host−guest FRET pair. *Chem. Commun.* **2019**, *55*, 671−674.
(43) Beatty, M. A.; Hof, F. Host−guest binding in water, salty water, and biofluids: general lessons for synthetic, bio-targeted molecular recognition. *Chem. Soc. Rev.* **2021**, *50*, 4812−4832.
(44) Kim, K. L.; Sung, G.; Sim, J.; Murray, J.; Li, M.; Lee, A.; Shrinidhi, A.; Park, K. M.; Kim, K. Supramolecular latching system based on ultrastable synthetic binding pairs as versatile tools for protein imaging. *Nat. Commun.* **2018**, *9*, 1712.
(45) Bockus, A. T.; Smith, L. C.; Grice, A. G.; Ali, O. A.; Young, C. C.; Mobley, W.; Leek, A.; Roberts, J. L.; Vinciguerra, B.; Isaacs, L.; Urbach, A. R. Cucurbit[7]uril−Tetramethylrhodamine Conjugate for Direct Sensing and Cellular Imaging. *J. Am. Chem. Soc.* **2016**, *138*, 16549−16552.
(46) Sun, C.; Wang, Z.; Yue, L.; Huang, Q.; Cheng, Q.; Wang, R. Supramolecular Induction of Mitochondrial Aggregation and Fusion. *J. Am. Chem. Soc.* **2020**, *142*, 16523−16527.
(47) Zheng, Z.; Geng, W.-C.; Li, H.-B.; Guo, D.-S. Sensitive fluorescence detection of saliva pepsin by a supramolecular tandem assay enables the diagnosis of gastroesophageal reflux disease. *Supramol. Chem.* **2021**, *33*, 80−87.
(48) Buryak, A.; Severin, K. A Chemosensor Array for the Colorimetric Identification of 20 Natural Amino Acids. *J. Am. Chem. Soc.* **2005**, *127*, 3700−3701.
(49) Wright, A. T.; Anslyn, E. V. Differential receptor arrays and assays for solution-based molecular recognition. *Chem. Soc. Rev.* **2006**, *35*, 14−28.
(50) Chen, J.; Hickey, B. L.; Wang, L.; Lee, J.; Gill, A. D.; Favero, A.; Pinalli, R.; Dalcanale, E.; Hooley, R. J.; Zhong, W. Selective discrimination and classification of G-quadruplex structures with a host−guest sensing array. *Nat. Chem.* **2021**, *13*, 488−495.
(51) Huang, W.-H.; Liu, S.; Zavalij, P. Y.; Isaacs, L. Nor-Seco-Cucurbit[10]uril Exhibits Homotropic Allosterism. *J. Am. Chem. Soc.* **2006**, *128*, 14744−14745.
(52) Prabodh, A.; Wang, Y.; Sinn, S.; Albertini, P.; Spies, C.; Spuling, E.; Yang, L.-P.; Jiang, W.; Bräse, S.; Biedermann, F. Fluorescence detected circular dichroism (FDCD) for supramolecular host−guest complexes. *Chem. Sci.* **2021**, *12*, 9420−9431.
(53) Assaf, K. I.; Nau, W. M. Cucurbiturils: from synthesis to high-affinity binding and catalysis. *Chem. Soc. Rev.* **2015**, *44*, 394−418.
(54) Barrow, S. J.; Kasera, S.; Rowland, M. J.; del Barrio, J.; Scherman, O. A. Cucurbituril-Based Molecular Recognition. *Chem. Rev.* **2015**, *115*, 12320−12406.
(55) Minaker, S. A.; Daze, K. D.; Ma, M. C. F.; Hof, F. Antibody-Free Reading of the Histone Code Using a Simple Chemical Sensor Array. *J. Am. Chem. Soc.* **2012**, *134*, 11674−11680.
(56) Biedermann, F.; Nau, W. M. Noncovalent Chirality Sensing Ensembles for the Detection and Reaction Monitoring of Amino Acids, Peptides, Proteins, and Aromatic Drugs. *Angew. Chem., Int. Ed.* **2014**, *53*, 5694−5699.
(57) Biedermann, F.; Hathazi, D.; Nau, W. M. Associative chemosensing by fluorescent macrocycle−dye complexes − a versatile enzyme assay platform beyond indicator displacement. *Chem. Commun.* **2015**, *51*, 4977−4980.
(58) Dsouza, R. N.; Pischel, U.; Nau, W. M. Fluorescent Dyes and Their Supramolecular Host/Guest Complexes with Macrocycles in Aqueous Solution. *Chem. Rev.* **2011**, *111*, 7941−7980.
(59) Sun, H.; Hunter, C. A.; Navarro, C.; Turega, S. Relationship between Chemical Structure and Supramolecular Effective Molarity for Formation of Intramolecular H-Bonds. *J. Am. Chem. Soc.* **2013**, *135*, 13129−13141.
(60) Ghosh, P. B.; Whitehouse, M. W. 7-chloro-4-nitrobenzo-2-oxa-1,3-diazole: a new fluorigenic reagent for amino acids and other amines. *Biochem. J.* **1968**, *108*, 155−156.
(61) Alnajjar, M. A.; Nau, W. M.; Hennig, A. A reference scale of cucurbit[7]uril binding affinities. *Org. Biomol. Chem.* **2021**, *19*, 8521−8529.
(62) Liu, S.; Ruspic, C.; Mukhopadhyay, P.; Chakrabarti, S.; Zavalij, P. Y.; Isaacs, L. The Cucurbit[n]uril Family: Prime Components for Self-Sorting Systems. *J. Am. Chem. Soc.* **2005**, *127*, 15959−15967.
(63) Rekharsky, M. V.; Yamamura, H.; Ko, Y. H.; Selvapalam, N.; Kim, K.; Inoue, Y. Sequence recognition and self-sorting of a dipeptide by cucurbit[6]uril and cucurbit[7]uril. *Chem. Commun.* **2008**, 2236−2238.
(64) Dong, N.; He, J.; Li, T.; Peralta, A.; Avei, M. R.; Ma, M.; Kaifer, A. E. Synthesis and Binding Properties of Monohydroxycucurbit[7]-uril: A Key Derivative for the Functionalization of Cucurbituril Hosts. *J. Org. Chem.* **2018**, *83*, 5467−5473.
(65) Atcher, J.; Moure, A.; Bujons, J.; Alfonso, I. Salt-Induced Adaptation of a Dynamic Combinatorial Library of Pseudopeptidic Macrocycles: Unraveling the Electrostatic Effects in Mixed Aqueous Media. *Chem. − Eur. J.* **2015**, *21*, 6869−6878.
(66) Sedgwick, A. C.; Brewster, J. T.; Wu, T.; Feng, X.; Bull, S. D.; Qian, X.; Sessler, J. L.; James, T. D.; Anslyn, E. V.; Sun, X. Indicator displacement assays (IDAs): the past, present and future. *Chem. Soc. Rev.* **2021**, *50*, 9−38.
(67) Stewart, S.; Ivy, M. A.; Anslyn, E. V. The use of principal component analysis and discriminant analysis in differential sensing routines. *Chem. Soc. Rev.* **2014**, *43*, 70−84.
(68) Harrison, E. E.; Carpenter, B. A.; St. Louis, L. E.; Mullins, A. G.; Waters, M. L. Development of "Imprint-and-Report" Dynamic Combinatorial Libraries for Differential Sensing Applications. *J. Am. Chem. Soc.* **2021**, *143*, 14845−14854.
(69) Mei, Y.; Zhang, Q.-W.; Gu, Q.; Liu, Z.; He, X.; Tian, Y. Pillar[5]arene-Based Fluorescent Sensor Array for Biosensing of Intracellular Multi-neurotransmitters through Host−Guest Recognitions. *J. Am. Chem. Soc.* **2022**, *144*, 2351−2359.
(70) Bland, J. M.; Altman, D. G. Multiple significance tests: the Bonferroni method. *BMJ* **1995**, *310*, 170.
(71) Lee, T.-C.; Kalenius, E.; Lazar, A. I.; Assaf, K. I.; Kuhnert, N.; Grün, C. H.; Jänis, J.; Scherman, O. A.; Nau, W. M. Chemistry inside molecular containers in the gas phase. *Nat. Chem.* **2013**, *5*, 376−382.
(72) Carroy, G.; Lemaur, V.; Henoumont, C.; Laurent, S.; De Winter, J.; De Pauw, E.; Cornil, J.; Gerbaux, P. Flying Cages in Traveling Wave Ion Mobility: Influence of the Instrumental Parameters on the Topology of the Host−Guest Complexes. *J. Am. Soc. Mass Spectrom.* **2018**, *29*, 121−132.
(73) Larriba, C.; Hogan, C. J. Free molecular collision cross section calculation methods for nanoparticles and complex ions with energy accommodation. *J. Comput. Phys.* **2013**, *251*, 344−363.
(74) Liu, Y.; Perez, L.; Mettry, M.; Easley, C. J.; Hooley, R. J.; Zhong, W. Self-Aggregating Deep Cavitand Acts as a Fluorescence Displacement Sensor for Lysine Methylation. *J. Am. Chem. Soc.* **2016**, *138*, 10746−10749.

(75) Zheng, Z.; Geng, W.-C.; Gao, J.; Wang, Y.-Y.; Sun, H.; Guo, D.-S. Ultrasensitive and specific fluorescence detection of a cancer biomarker via nanomolar binding to a guanidinium-modified calixarene. *Chem. Sci.* **2018**, *9*, 2087−2091.
(76) Anzenbacher, J. P.; Lubal, P.; Buček, P.; Palacios, M. A.; Kozelkova, M. E. A practical approach to optical cross-reactive sensor arrays. *Chem. Soc. Rev.* **2010**, *39*, 3954−3979.
(77) Lee, B.; Scopelliti, R.; Severin, K. A molecular probe for the optical detection of biogenic amines. *Chem. Commun.* **2011**, *47*, 9639−9641.
(78) Beatty, M. A.; Borges-González, J.; Sinclair, N. J.; Pye, A. T.; Hof, F. Analyte-Driven Disassembly and Turn-On Fluorescent Sensing in Competitive Biological Media. *J. Am. Chem. Soc.* **2018**, *140*, 3500−3504.
(79) Miskolczy, Z.; Megyesi, M.; Sinn, S.; Biedermann, F.; Biczók, L. Simultaneous analyte indicator binding assay (SBA) for the monitoring of reversible host−guest complexation kinetics. *Chem. Commun.* **2021**, *57*, 12663−12666.
(80) Prabodh, A.; Sinn, S.; Grimm, L.; Miskolczy, Z.; Megyesi, M.; Biczók, L.; Bräse, S.; Biedermann, F. Teaching indicators to unravel the kinetic features of host−guest inclusion complexes. *Chem. Commun.* **2020**, *56*, 12327−12330.
(81) Manoni, F.; Fornasiero, L.; Ercolin, M.; Tinello, A.; Ferrian, M.; Valverde, S.; Gessoni, G. Laboratory diagnosis of renal failure: urine conductivity and tubular function. *Minerva Urol. Nefrol.* **2009**, *61*, 17−20.

https://doi.org/10.1021/jacs.2c01520
J. Am. Chem. Soc. 2022, 144, 13084−13095